Aggregation of Granulocyte Colony Stimulating Factor under Physiological Conditions: Characterization and Thermodynamic Inhibition†

Sampathkumar Krishnan,‡ Eva Y. Chi,§ Jonathan N. Webb,|| Byeong S. Chang,⊥ Daxian Shan,⊥ Merrill Goldenberg,⊥ Mark C. Manning,‡ Theodore W. Randolph,§ and John F. Carpenter*,‡

Department of Pharmaceutical Sciences, School of Pharmacy, University of Colorado Health Sciences Center, Denver, Colorado 80262, Department of Chemical Engineering, University of Colorado, Boulder, Colorado 80309, Integrated Biosystems, Napa, California 94558, and Amgen, Inc., Thousand Oaks, California 91320

Received November 1, 2001; Revised Manuscript Received February 13, 2002

ABSTRACT: We have investigated the aggregation of recombinant human granulocyte colony stimulating factor (rhGCSF), a protein that rapidly aggregates and precipitates at pH 6.9 and 37 °C. We observed that native monomeric rhGCSF reversibly forms a dimer under physiological conditions and that this dimeric species does not participate in the irreversible aggregation process. Sucrose, a thermodynamic stabilizer, inhibits the aggregation of rhGCSF. We postulate that sucrose acts by reducing the concentration of structurally expanded species, consistent with the hypothesis that preferential exclusion favors most compact species in the native state ensemble. Thermodynamic stability data from unfolding curves and hydrogen−deuterium exchange experimental results support the above hypothesis. Thus, the strategy of stabilizing the native state of the protein under physiological conditions using thermodynamic stabilizers, especially ligands binding with high affinity to the native state, is expected to protect against protein aggregation occurring under such nonperturbing solution conditions.

Protein aggregation and subsequent deposition as insoluble fibrils or amorphous precipitates is responsible for a number of diseases such as Alzheimer's disease, Parkinson's disease, Huntington's disease, and systemic amyloidosis (*1*−*5*). Protein aggregation is also a dominant degradation pathway for therapeutic proteins, potentially occurring during all phases of production, purification, shipping, storage, and administration (*6*−*8*). Protein aggregates in parenterally delivered protein formulations can cause adverse reactions in patients ranging from immune responses to anaphylactic shock (*6*−*8*). To develop rational strategies to prevent protein aggregation in vitro and in vivo, we must understand better the structural perturbations that lead to aggregation and the influence of exogenous stabilizers on the initial steps of the aggregation pathway.

In this work, we consider aggregates to be assemblies of proteins that are non-native. If the assemblies are large enough, solubility limits may be exceeded, and the aggregates may precipitate. These precipitates typically contain a high level of non-native intermolecular β-sheet structure (*9*). Research to date suggests that most protein aggregates are formed from partially unfolded molecules, which are in equilibrium with the native state (*10*, *11*). Perturbing solution conditions (e.g., acid pH, high temperature, or presence of nondenaturing concentrations of chaotropes) shift the equilibrium toward partially unfolded protein molecules. Thus, these conditions are often used for in vitro aggregation studies to initiate aggregation and to increase the level of partially unfolded species (e.g., molten globules) sufficiently to allow their structural characterization by spectroscopic techniques (*12*, *13*). In terms of human diseases, perturbing solvent environments can be found in the renal medulla of the kidney, which contains high concentrations of urea (*14*), as well as in the lysozome, in which the pH is near 4 (*15*).

It is often assumed that the structural perturbation found under conditions used for spectroscopic analyses of partially unfolded species is similar or identical to that causing aggregation in vivo and in commercial formulations of therapeutic proteins. However, protein aggregation also occurs, albeit more slowly, under conditions greatly favoring the native state (e.g., physiological conditions: 37 °C at neutral pH) in vivo and in vitro (*16*−*20*). Recently it has been proposed that under these conditions aggregation proceeds through a transition state species within the native state ensemble that is only slightly perturbed in structure relative to the most compact species (*16*, *21*). Even though the transition state is part of the native ensemble, the final aggregates have dramatically perturbed structures containing a high level of non-native intermolecular β-sheet. To date, this proposal has only been tested for a single protein, interferon-γ, for which nondenaturing concentrations of GdnHCl[1] were used to foster aggregation (*16*, *21*). In the present work, we studied rhGCSF to determine if the aggregation mechanism and resulting structural changes are

† This research was supported by grants from the National Science Foundation (BES-9816975) and Amgen, Inc. E.Y.C. was supported by a NSF Graduate Fellowship.

* To whom correspondence should be addressed at the Department of Pharmaceutical sciences, School of Pharmacy, University of Colorado Health Sciences Center, Denver, CO 80262. Phone: 303-315-6074, Fax: 303-315-6281, Email: john.carpenter@uchsc.edu.

‡ Department of Pharmaceutical Sciences, University of Colorado Health Sciences Center.

§ Department of Chemical Engineering, University of Colorado.

|| Integrated Biosystems.

⊥ Amgen, Inc.

10.1021/bi012006m CCC: $22.00
Published on Web 04/26/2002

similar under conditions greatly favoring the native state, without addition of specific perturbing agents (e.g., GdnHCl).

Nonspecific thermodynamic stabilizers (e.g., sucrose) have been shown to inhibit aggregation of both proteins involved in human diseases (e.g., immunoglobulin light chains) and therapeutic proteins (*22*−*24*). There is also great interest in the roles that such solutes can play in protein stabilization from the viewpoint of adaptation of organisms to extreme environments, for which a critical component is the accumulation of relatively high concentrations of stabilizing solutes ("osmolytes") such as sucrose (*25*, *26*). Timasheff and colleagues have defined rigorously the nonspecific mechanism for thermodynamic stabilization of proteins by solutes (*27*−*29*). These substances are preferentially excluded from the protein's surface, concomitant with an increase in the protein chemical potential. The magnitude of preferential exclusion and the increase in protein chemical potential are directly dependent on the solvent-exposed surface area of the protein. Because the denatured state has a greater solvent-exposed surface area than the native state, the degree of preferential exclusion and the increase in chemical potential are greater for the denatured than for the native state. Thus, the free energy barrier between the states is increased and the native state is stabilized.

This thermodynamic mechanism can also be used to explain how compounds such as sucrose can inhibit protein aggregation. If a partially unfolded species is required for aggregation, then addition of an excluded solute can inhibit aggregation by shifting the equilibrium to favor the more compact states within the native ensemble and reduce the concentration of the aggregation-competent intermediate (*16*, *19*). Thus, sucrose can be used as a tool to understand protein aggregation pathways (*16*, *17*).

The aims of the present study were to characterize the aggregation of recombinant human granulocyte colony stimulating factor (rhGCSF) under physiological conditions, along with the structural perturbations taking place in the protein, and to determine the effect of sucrose on rhGCSF aggregation kinetics, thermodynamic stability, and hydrogen−deuterium exchange rates. rhGCSF is a 19 kDa monomeric protein belonging to the four-α-helical bundle family of growth factors (*30*−*32*). In the commercial therapeutic formulation (0.3−0.5 mg/mL, pH 4.0, with 5% sorbitol and 0.004% polysorbate-80), rhGCSF has a shelf life of more than 2 years at 2−8 °C, during which it maintains native α-helix structure and is greatly resistant to aggregation (*30*−*32*). However, as we document in this study, rhGCSF aggregates rapidly in phosphate-buffered saline at pH 6.9 and 37 °C.

EXPERIMENTAL PROCEDURES

Materials. Pharmaceutical quality rhGCSF was produced and purified (>99%) at Amgen, Inc. (Thousand Oaks, CA). The protein was obtained as a stock solution of 4 mg/mL in aqueous HCl solution at pH 3.25, and stored at 4 °C. Sodium phosphate, sodium chloride, and guanidine hydrochloride were purchased from Sigma. High purity sucrose was purchased from Pfanstiehl Laboratories. Deuterium oxide (99.9% D) was purchased from Aldrich. All chemicals were of reagent grade or higher quality.

Aggregation Conditions. Unless otherwise indicated, the stock solution of rhGCSF was diluted to a final concentration of 1.5 mg/mL in phosphate-buffered saline (PBS: 10 mM sodium phosphate and 150 mM sodium chloride at pH 7.0) using concentrated solutions of sucrose (prepared in PBS) to yield final concentrations of 0, 0.25, 0.5, 0.75, or 1.0 M sucrose. The protein solutions (1 mL) were incubated at 37 °C in 1.5 mL polypropylene Eppendorf tubes without agitation. Samples were prepared and incubated in triplicate. Aliquots (65 μL) from these solutions were collected at regular intervals over a 5 day period. Before removing aliquots, the contents of the Eppendorf tube were resuspended by gently moving the solution into and out of a pipet tip, twice. The collected aliquots were centrifuged for 10 min to remove any insoluble precipitate. The supernatant was analyzed using SE-HPLC (HP1090 system with a diode array detector and a 0.2 μm filter precolumn) by injecting 50 μL onto a Tosohaas TSK-GEL G2000SW$_{XL}$ column. The mobile phase was 100 mM sodium phosphate (pH 7.0), at a flow rate of 0.6 mL/min. The column eluate was monitored at 215 nm. Peak areas in the chromatogram were used to quantify the amounts of monomer and dimer in incubated samples. The amount of protein present was calculated by dividing the measured peak area by the peak area for an unincubated control sample (1.5 mg/mL) of rhGCSF and multiplying the result by 100. The insoluble protein fraction was calculated as the difference between the total protein present before incubation and the soluble protein remaining after incubation, based on peak areas in the respective chromatograms. In preliminary experiments (data not shown), the values for soluble protein obtained by this method were corroborated by chemical determination (bicinchoninic acid assay) of total soluble protein in the sample supernatants. The molecular weight of protein species appearing in the chromatogram was analyzed using light scattering and refractive index detectors (model 300 TDA, Viscotek).

Reversibility of Dimer Formation. To determine if the dimer formed during incubation at 37 °C could be reversibly dissociated upon dilution, 2 mg/mL rhGCSF was incubated at 37 °C and pH 6.9 for 2 h, and then diluted. Samples were diluted with phosphate-buffered saline (PBS: 10 mM sodium phosphate, 150 mM NaCl, pH 7.0) to 0.5, 1.0, and 1.5 mg/mL protein and incubated at room temperature. Aliquots of the sample were analyzed using SE-HPLC prior to and 2, 4, and 5 h after dilution.

In a second test, 16 mg of rhGCSF was dissolved in 200 μL of water, pH 3.0. The solution was injected in a SE-HPLC system (running buffer: 25 mM sodium phosphate, 125 mM NaCl in water, pH 6.9) at room temperature. Injection of this relatively high concentration (80 mg/mL) of rhGCSF resulted in the formation of dimers during chromatography as the protein equilibrated with the running buffer. The presence of dimer was indicated by the appearance of a distinct peak in the chromatogram at an elution volume for dimeric rhGCSF. Dimer formation was not detected if lower concentrations of rhGCSF (e.g., 1.5 mg/mL) are prepared at pH 3.0 and injected onto the SE-HPLC column (data not shown).

[1] Abbreviations: rhGCSF, recombinant human granulocyte colony stimulating factor; GdnHCl, guanidine hydrochloride; SE-HPLC, size exclusion high-performance liquid chromatography; PBS, phosphate-buffered saline; DLS, dynamic light scattering; CD, circular dichroism; IR, infrared; UV, ultraviolet; H−D, hydrogen−deuterium; TEM, transmission electron microscopy.

Alternative methods to prepare sufficient quantities of dimer, such as dialyzing 80 mg/mL rhGCSF against PBS or directly diluting a concentrated rhGCSF stock into PBS, invariably resulted in massive precipitation of the protein. Thus, we chose to use direct injection of the pH 3.0 rhGCSF solution at relatively high protein concentration (in water) onto the column as a preparative method for dimers. Dimer fractions were pooled from multiple injections, and then were concentrated 2-fold using a Microcon YM-10 centrifugal filter. The final dimer solution contained 0.14 mg/mL rhGCSF in 25 mM sodium phosphate, 125 mM NaCl, pH 6.9. SE-HPLC analysis of the concentrated, pooled fractions showed that 91% of the rhGCSF was dimeric and 9% was monomeric. Aliquots (70 μL) of this solution were placed in sample vial inserts and incubated at 37 °C. At various time points, samples were withdrawn, and analyzed for monomeric and dimeric rhGCSF by SE-HPLC.

Reaction Rate Order Determination for Aggregation. Protein solutions at 0.5, 1, 2, and 4 mg/mL were prepared in PBS and incubated at 37 °C. Samples were collected at regular intervals, centrifuged, and analyzed by SE-HPLC. The concentration of monomeric protein was plotted against time to obtain the initial rate of the loss of monomer at various protein concentrations. The order of the reaction was determined from the slope of a log−log plot of initial rate versus rhGCSF concentration.

Second-Derivative UV Spectroscopy. UV absorbance scans (from 190 to 600 nm) of the monomer and dimer peaks on the SE-HPLC chromatogram were obtained from the HP1090 liquid chromatography system's diode array detector (*33*). The data were then processed using BOMEM-Grams software. The data were interpolated, and the second-derivative spectrum was calculated using a Savitzky−Golay function. The second-derivative UV spectra of *N*-acetyltyrosinamide and *N*-acetyltryptophanamide in PBS buffer were also obtained for comparison purposes. To obtain second-derivative UV spectra for protein precipitates, a UV−visible spectrophotometer (Perkin-Elmer Lambda 3B model) was used. To remove soluble components, the precipitate was centrifuged and resuspended in PBS 3 times before acquiring UV spectra. The process of centrifugation and resuspension of the precipitated protein resulted in sufficient reduction in aggregate particle size that the material remained suspended during the acquisition (ca. 5 min) of the UV spectrum. This method led to adequate absorbance values (>0.1 absorbance unit) for calculating high-quality and reproducible second-derivative spectra of the precipitated protein. Light scattering contributions are negligible in second-derivative UV spectra and do not alter the signal obtained from protein absorbance (*21*, *33*). Replicate spectra of precipitated protein samples were indistinguishable (data not shown). Appropriate blank corrections for buffer alone were performed. The data were processed as above.

Circular Dichroism Spectroscopy and Unfolding Studies. Far-UV CD (Aviv 62DS) spectra were collected using a 1 mm path-length cell at a protein concentration of 0.1 mg/mL. Appropriate subtractions of the buffer spectra from the protein spectra were performed. Thermal unfolding and GdnHCl-induced unfolding experiments (25 °C) were performed with the protein in PBS with 0, 0.25, 0.5, 0.75, and 1.0 M sucrose. The solutions for guanidine-induced unfolding were allowed to equilibrate for 2 days at room temperature, and CD spectra were recorded at room temperature. Unfolding was monitored at 222 nm (α-helix region) because the difference in signal between native and denatured protein is greatest at this wavelength. The unfolding midpoint (C_m) was calculated from the GdnHCl unfolding curve by nonlinear regression analysis (*34*, *35*). The free energy of unfolding, ΔG_{unf}, was determined by the linear extrapolation method (*36*, *37*).

We also attempted to use urea to study unfolding of rhGCSF employing CD spectroscopy, as described above for GdnHCl-induced unfolding. Due to limited solubility of urea in the presence of sucrose and the relatively high C_m for urea-induced unfolding, we were only able to obtain complete unfolding curves in 0, 0.25, and 0.5 M sucrose. The free energy of unfolding was determined by the linear extrapolation method (*36*, *37*).

For thermal unfolding, the sample temperature was increased at 2 °C/min, and the CD signal at 222 nm was monitored. The same heating rate, which was highly reproducible (±0.06 °C/min), was used for all samples. Fraction folded protein was calculated as previously described (*36*, *37*) and plotted against temperature to give unfolding curves. The curves for all samples tested had a single, highly cooperative transition from native to unfolded protein, centered at the apparent T_m (Figure 5B).

ΔS_m and ΔH_m, the molar changes in entropy and enthalpy at the melting point, respectively, were calculated from van't Hoff analysis (*36*, *37*). The r^2 values for the regressed lines—for samples analyzed at each sucrose concentration—all had values of 0.9999, indicating that probably only unfolding of the protein is contributing to the observed change in CD signal with temperature. Thermal unfolding was 15% reversible when samples were heated to approximately 10 °C above the melting point. However, when a separate sample was heated to the melting point and then recooled to 25 °C, thermal unfolding was 60% reversible.

The free energy of unfolding (ΔG_{unf}) at 310 K was calculated using the formula:

$$\Delta G_{unf}(T) = \Delta H_m(1 - T/T_m) - \Delta C_p[T_m - T + T^* \ln (T/T_m)] \quad (1)$$

where T is the temperature and T_m is the apparent melting point from thermal unfolding curves. The change in heat capacity upon melting (ΔC_p) was estimated, based on the number of amino acid residues in rhGCSF, to be 2.088 kcal K^{-1} mol^{-1} (*38*).

Infrared Spectroscopy. A concentrated solution of the stock of unincubated rhGCSF was prepared by using a Centricon centrifugal concentrator (model-10). This solution was then diluted with 2.5-times-concentrated PBS to yield a final protein concentration of 8 mg/mL in PBS and used to obtain the infrared (IR) spectrum of the native protein. The precipitate of the protein collected from samples after incubation at 37 °C was also analyzed. Sample preparation, spectral acquisition, and data analysis were performed as described by Kim et al. (*20*).

Hydrogen−Deuterium (H−D) Exchange. Deuterated buffer and sucrose solutions were prepared by lyophilizing solutions and rehydrating them to original volumes with deuterium oxide as described previously (*17*, *39*). A 50 μL aliquot of the concentrated protein (30 mg/mL) was diluted with 150

Table 1: Monomer−Dimer Equilibrium and Aggregation Rate Constants for rhGCSF Aggregation as a Function of Sucrose Concentration[a]

[sucrose] (M)	ν (μmol L^{-1} day^{-1})	K_D (L/mol)[b]	viscosity[c] (μ) at 37 °C (cP)
0	7.3 ± 0.6	157 ± 14	0.697
0.25	4.8 ± 0.7	180 ± 11	0.87
0.5	2.8 ± 1.5	176 ± 10	1.15
0.75	1.4 ± 1.3	178 ± 21	1.36
1	0.7 ± 0.2	185 ± 14	1.79

[a] The calculated values represent mean ± SD for triplicate samples. [b] K_D is the apparent monomer−dimer equilibrium constant (determined under SE-HPLC column conditions) and is the average of [dimer]/[monomer]^2 for ratios obtained at each time point. [c] Values for viscosity, in units of centipoise, were extrapolated from values of viscosity of water at different temperatures and viscosity of aqueous sucrose solutions at different concentrations, obtained from CRC (Handbook of Chemistry and Physics, 80th ed., 1999−2000).

μL of deuterated PBS (pD 6.6) or PBS/sucrose solutions. The final protein solution was immediately placed in the sample cell, and IR spectra were obtained over a 24 h period. A 64-scan interferogram was collected for the spectra acquired during the first 30 min, and for later time points, 128-scan interferograms were collected. Spectra were processed, and the extent of H−D exchange reaction was determined by amide II/I ratios as described previously (*40*, *17*, *19*).

Transmission Electron Microscopy. The structure of precipitates of rhGCSF, formed during incubation 37 °C and pH 6.9, was studied by TEM (Philips CM-10). The sample was placed on a grid (460-thin bar copper mesh) and negatively stained using 2% uranyl acetate solution. The samples were then air-dried before analysis at 50 000−100 000×.

RESULTS

Inhibition of the Aggregation of the Protein. During incubation at pH 6.9 and 37 °C in PBS, there was a progressive loss of monomeric rhGCSF, with only 4% remaining after 5 days (Figure 1A). An acceleration of the rate over time is apparent in samples containing 0.5 M or less sucrose. SE-HPLC (Figure 1B) and light-scattering detection (data not shown) indicated that a dimer formed early in the incubation. After reaching a maximum level (3.5% of total protein), dimer levels gradually declined to less than 0.2% (Figure 1B). An increase in insoluble protein aggregate level was concomitant with the decrease in monomeric rhGCSF (Figure 1C). TEM documented that precipitates were amorphous aggregates (data not shown).

Increasing concentrations of sucrose progressively inhibited the rate of loss of monomeric protein and the formation of insoluble aggregates (Figure 1, Table 1). The peak dimer levels obtained during the early period of the incubation were indistinguishable for all sucrose concentrations tested (Figure 1B). During subsequent incubation, increasing sucrose concentration progressively decreased the loss of dimer. Furthermore, the ratio of [dimer]/[monomer]^2 remained essentially constant at 175 L/mol for all solution conditions from 2 h to 5 days of incubation (Table 1).

Figure 2A shows that dimers formed during incubation dissociated upon dilution. The extent of dissociation increased with increasing dilution. In all cases, the decrease

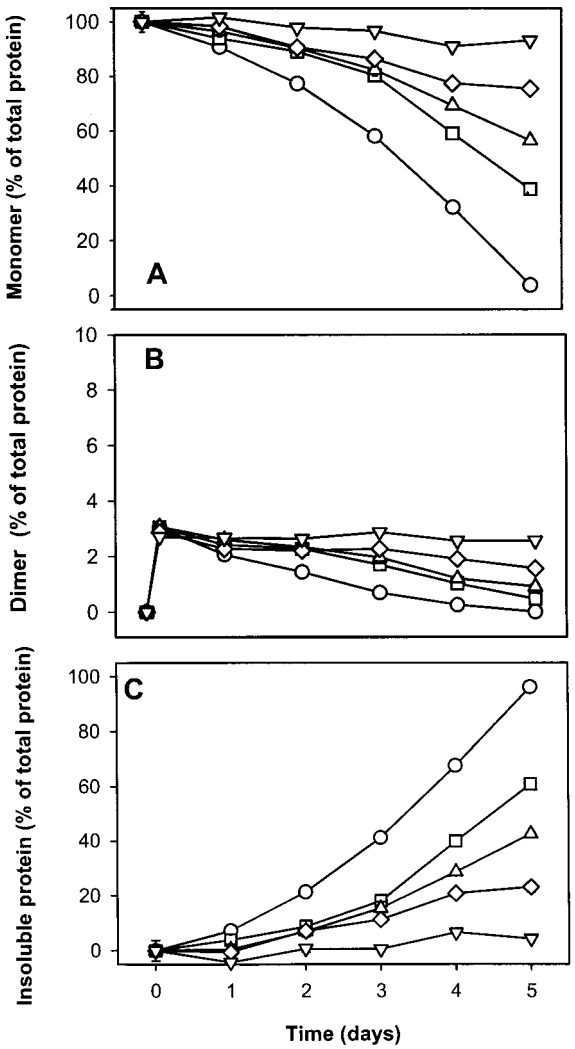

FIGURE 1: Size exclusion chromatographic analysis of rhGCSF aggregation. (A) Percentage of monomer remaining in solution as a function of time. Increasing concentrations of sucrose (circles, 0 M; squares, 0.25 M; upward triangles, 0.5 M; diamonds, 0.75 M; downward triangles, 1 M) inhibited the loss of monomer from solution from nearly 96% loss in 0 M sucrose to 7% loss in 1 M sucrose solution over a 5 day period. (B) Formation of dimer as a percentage of the total initial protein. (C) Percentage of insoluble aggregate formation as a function of time. In most cases, error bars (mean ± SD) are smaller than the symbols.

in dimer was accompanied by an increase in monomer levels (data not shown). Dimer fractions purified by SE-HPLC dissociated to monomers (Figure 2B), with a time constant of 1.6 h. The total peak areas seen in the SE-HPLC analysis (monomer + dimer) remained constant after 8 h of incubation at 37 °C (data not shown), indicating that no aggregation could be detected.

The aggregation reaction order in the absence of sucrose was determined from the slope of a log−log plot of the initial rates of protein aggregation versus protein concentration (Figure 3). The slope (2.17 ± 0.09) shows that initial aggregation of rhGCSF was a second-order process in monomer concentration. At later times, the acceleration evident in Figure 1A suggests that the observed reaction order increased with time.

Structural Changes Accompanying Aggregation. The second-derivative IR spectra of native and precipitated rhGCSF are shown in Figure 4A. The secondary structure

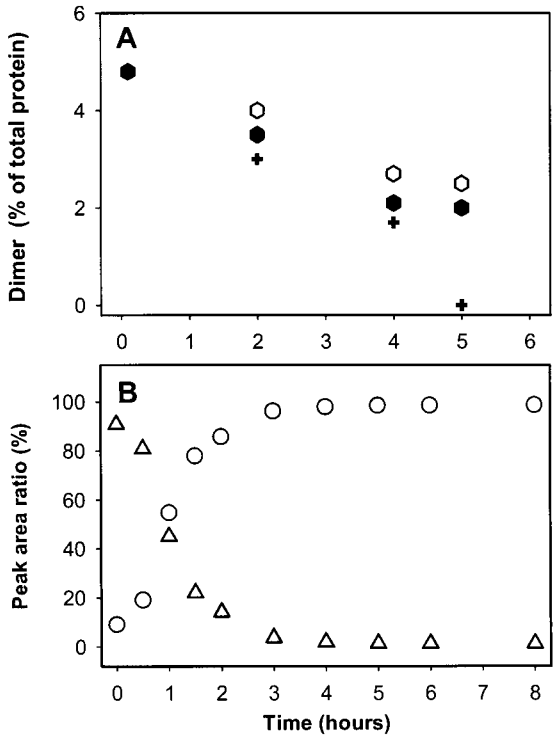

FIGURE 2: Reversibility of dimer. (A) Dimer formed in 2 mg/mL rhGCSF solution after 2 h of incubation at pH 6.9 and 37 °C was diluted to 1.5 (closed hexagons), 1 (open hexagons), and 0.5 mg/mL (crosses) solutions. The dimer levels dropped for all the above protein concentrations on incubation for 5 h. (B) Purified dimer (total rhGCSF concentration 0.14 mg/mL) was incubated in 25 mM phosphate, 125 mM NaCl, pH 6.9, for various times, and then rechromatographed by SE-HPLC and analyzed for monomer (circles) and dimer (triangles).

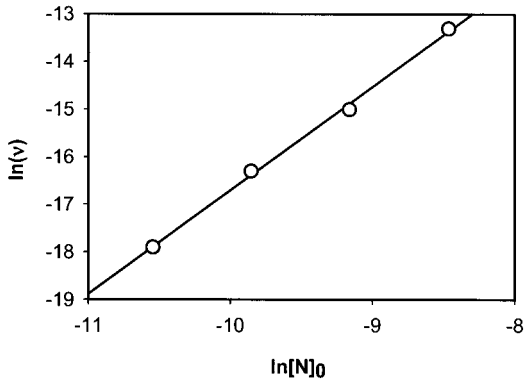

FIGURE 3: Determination of the order of the aggregation reaction of rhGCSF. rhGCSF at various concentrations was incubated at pH 6.9 and 37 °C. The initial loss of rhGCSF from solution was determined using SE-HPLC analysis. The figure shows the natural logarithm of ν (initial rate of aggregation in mol L^{-1} h^{-1}) vs the natural logarithm of N_o (initial rhGCSF concentration in mol/L).

of the native protein is predominantly α-helical, as evidenced by the dominant band at 1656 cm^{-1}. Addition of 1 M sucrose did not alter, detectably, the IR spectrum for the native protein (data not shown). The precipitated protein still retained some α-helical structure but had a high level of intermolecular β-sheet, as evidenced by the strong bands at 1620 and 1695 cm^{-1}.

Second-derivative UV absorbance spectroscopy was used to detect tertiary conformational changes involving the microenvironments of aromatic amino acids (*41*). The mutual

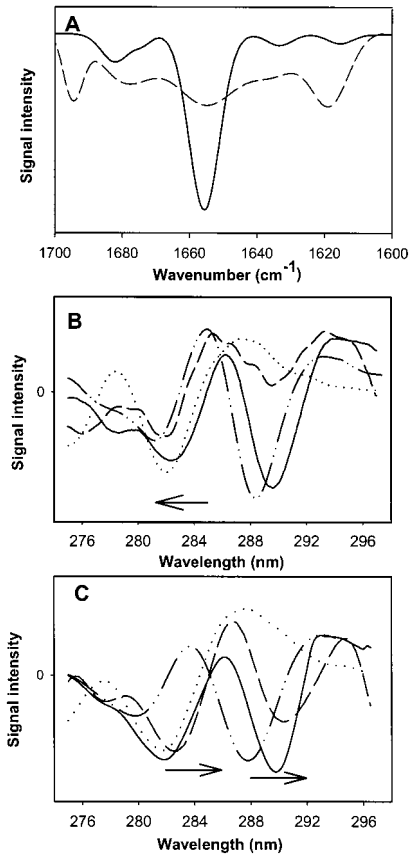

FIGURE 4: Structural changes of rhGCSF during aggregation. (A) Second-derivative IR spectra of native (solid line) and precipitated protein (dashed line). (B) Second-derivative UV spectra of the native protein (solid line), aggregate (dashed line), *N*-acetyltryptophanamide (dash and dotted line), and *N*-acetyltyrosinamide (dotted line). (C) Second-derivative UV spectrum of the dimer (dashed line) with respect to the second-derivative UV spectra of native protein, *N*-acetyltryptophanamide (dash and dotted line), and *N*-acetyltyrosinamide (dotted line). The direction of the arrows indicates the shift of minima in the spectrum of the aggregate (insoluble/dimer) with respect to the native protein.

interference between the second-derivative bands of tyrosine and tryptophan, evaluated in terms of the ratio between peak-to-peak distances, has been utilized for simultaneous determination of solvent exposure of these two residues (*42*, *43*). rhGCSF has two tryptophan and three tyrosine residues per molecule (*30*−*32*). To assess the microenvironment of these residues in rhGCSF, we compared the second-derivative UV spectrum of the protein with those of *N*-acetyltryptophanamide and *N*-acetyltyrosinamide in PBS (*33*, *41*−*43*). A red shift in the protein spectrum relative to the spectra for these compounds denotes increased hydrophobic environment of the corresponding residues in the protein (*42*). The tyrosine second-derivative UV spectrum has a minimum around 283 nm and maximum around 287 nm, whereas tryptophan has a minimum at 290 nm and maximum at around 295 nm. The tryptophan absorbance minima of native rhGCSF and the precipitated protein are both red-shifted versus *N*-acetyltryptophanamide by nearly 1.3 nm (Figure 4B). Thus, tryptophan in the native and precipitated protein is in a hydrophobic environment.

Figure 4B shows that the tyrosine absorbance minimum of native rhGCSF is slightly red-shifted compared to that of *N*-acetyltyrosinamide, indicating that the tyrosine residues

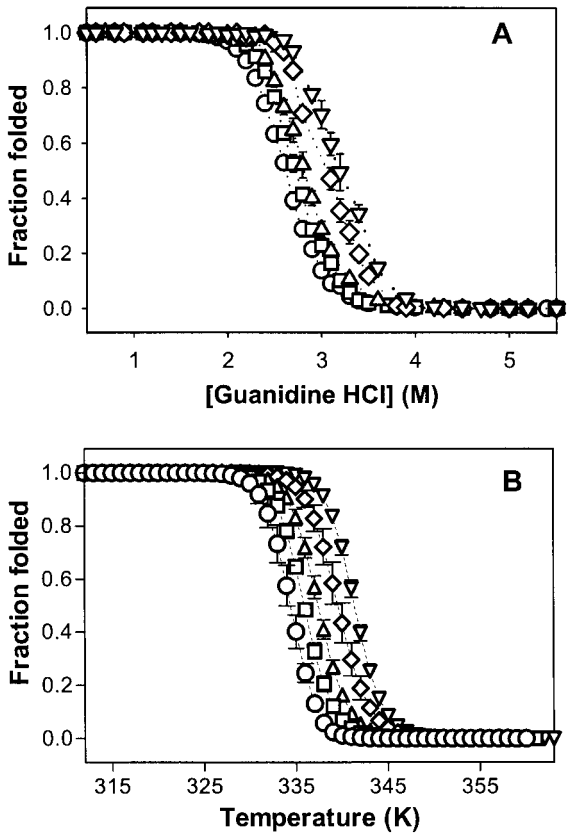

FIGURE 5: Guanidine hydrochloride (A) and thermal (B) unfolding curves for rhGCSF. Increasing concentrations of sucrose (circles, 0 M; squares, 0.25 M; upward triangles, 0.5 M; diamonds, 0.75 M; downward triangles, 1 M) shift the midpoint of the unfolding curves to high GdnHCl concentrations. Data points represent the mean ± SD for triplicate samples.

are in a hydrophobic environment. In contrast, the value for the precipitated protein is essentially the same as that for *N*-acetyltyrosinamide in PBS, indicating that the tyrosine residues in the precipitated rhGCSF are solvent-exposed.

Figure 4C shows the second-derivative UV spectrum for the dimer, observed in the chromatogram of a sample of rhGCSF after 1.5 h of incubation at pH 6.9. The red shifts versus *N*-acetyltryptophanamide and *N*-acetyltyrosinamide in PBS for tryptophan and tyrosine in the spectrum of the dimer are greater than those for the monomer. The tyrosine and tryptophan of the dimer are less solvent-exposed compared to the residues in monomeric protein.

Thermodynamic Parameters from Unfolding Experiments. Far-UV CD spectra of the protein in buffer and 1 M sucrose were indistinguishable with maximum ellipticity at 222 and 208 nm, indicative of α-helical structure (data not shown). GdnHCl-induced unfolding of the protein was performed using 0, 0.25, 0.5, 0.75, and 1.0 M sucrose solutions in PBS (Figure 5A). Unfolding was 85−90% reversible upon dilution of GdnHCl (data not shown). The midpoint of the unfolding transition shifted to higher concentrations of GdnHCl with increasing concentrations of sucrose (Figure 5A, Table 2). Similarly, the C_m values for urea-induced unfolding in 0, 0.25, and 0.50 M sucrose were 5.76, 6.02, and 6.26, respectively. The method for determining ΔG_{unf} described by Pace et al. (*36*, *37*) requires a linear extrapolation of ΔG_{unf} versus denaturant concentration, assuming that denaturant activity and concentration are interchangeable. When comparing different proteins or mutations of a given protein in a single solvent system, this assumption is generally reasonable. However, we observed that 1 M sucrose reduced the solubility (i.e., increased chemical potential) of urea by about 40% (data not shown). The activity of the denaturant is greatly increased by the presence of sucrose, which then can counteract the direct stabilization of the protein by sucrose. Even though we found that sucrose did increase C_m, ΔG_{unf} values estimated by the linear extrapolation method in sucrose solutions containing urea and GdnHCl were not statistically different from values for the protein in PBS alone (data not shown). Thus, in the presence of sucrose, we were unable to estimate the thermodynamic stability of rhGCSF using urea- or GdnHCl-induced unfolding.

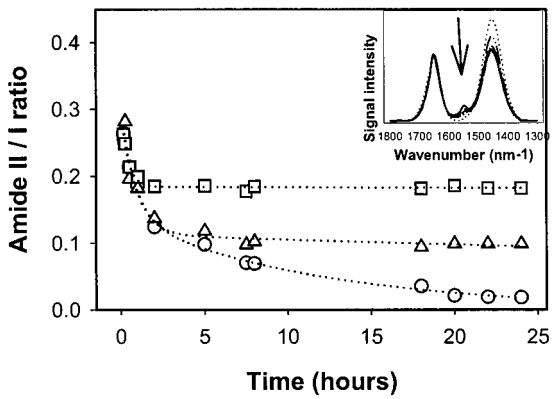

FIGURE 6: Effect of sucrose on the H−D exchange of rhGCSF determined using IR spectroscopy. The figure presents the change in amide II/I ratio of the IR absorbance spectra (inset) as a function of time of deuteration. Increasing concentrations of sucrose (circles, 0 M; upward triangles, 0.5 M; squares, 1 M) decreased the H−D exchange rate. The arrow in the inset points to the direction of the change in amide II with H−D exchange.

To avoid limitations imposed by chaotrope-induced unfolding, we tested thermal unfolding, which documented that sucrose increased the stability of the protein (Figure 5B, Table 2). For example, ΔG_{unf} at 37 °C increased in the presence of sucrose by almost 3 kcal/mol in a 1.0 M sucrose solution. The presence of sucrose increases the enthalpy of melting, which was compensated partially by an increase in the entropy of melting (Table 2).

H−D Exchange for rhGCSF. H−D exchange for rhGCSF in 0, 0.5, and 1 M sucrose in PBS was monitored with IR spectroscopy at room temperature over 24 h. Due to the formation of N−D from N−H, there is a decrease in the amide II/amide I ratio as a function of time of exposure to D_2O (Figure 6). Increasing concentrations of sucrose slowed the exchange. It has been previously been shown (*44*) that 1 M sucrose does not affect the intrinsic H−D exchange rate of poly-DL-alanine. Thus, the sucrose-induced attenuation of H−D exchange in proteins is not due to a direct effect of sucrose on the exchange process; rather, it results from the compaction of the time-average protein conformation by the sugar (*17*, *19*, *40*, *44*).

DISCUSSION

Structural Transitions Accompanying Aggregation. Under conditions where the native state is greatly favored thermodynamically (e.g., pH 6.9 and 37 °C, where ΔG_{unf} is 7.1

Table 2: Thermodynamic Parameters of rhGCSF from GdnHCl and Thermal Unfolding Curves[a]

[sucrose] (M)	C_m[b] (M)	T_m[c] (K)	ΔS_m[d] (kcal mol^{-1} K^{-1})	ΔH_m[e] (kcal/mol)	ΔG_{unf}(310 K)[f] (kcal/mol)
0	2.60 ± 0.02	334.1 ± 2.0	0.38 ± 0.02	127.0 ± 6.3	7.12 ± 0.35
0.25	2.72 ± 0.02	336.0 ± 1.3	0.39 ± 0.02	131.0 ± 7.9	8.04 ± 0.48
0.5	2.87 ± 0.06	336.7 ± 2.0	0.40 ± 0.02	134.7 ± 6.7	8.41 ± 0.41
0.75	3.07 ± 0.13	338.5 ± 2.1	0.41 ± 0.02	138.8 ± 12.8	9.62 ± 0.88
1.0	3.21 ± 0.07	341.2 ± 1.8	0.42 ± 0.03	143.3 ± 8.6	10.04 ± 0.60

[a] The calculated values represent mean ± SD for triplicate samples. [b] C_m is the midpoint of transition of the GdnHCl unfolding curve determined using complex sigmoid, nonlinear regression analysis (*34*, *35*). [c] T_m is the apparent melting point from the thermal unfolding curves. [d] ΔS_m is the slope of ΔG_{unf} (kcal/mol) plotted versus temperature (K). [e] ΔH_m calculated as $T_m \times \Delta S_m$. [f] The free energy of thermal unfolding, ΔG_{unf}(310 K), was calculated using eq 1. The change in heat capacity, ΔC_p, was calculated using the relationship (*38*): ΔC_p = number of amino acids × 12 cal deg^{-1} mol^{-1} residue^{-1} (2.088 kcal deg^{-1} mol^{-1} for rhGCSF).

kcal/mol), rhGCSF rapidly aggregates and forms amorphous precipitates with high intermolecular β-sheet content and greater solvent exposure of tyrosine residues than in the native monomeric protein. The degree of structural perturbation resulting from aggregation is remarkably similar to that noted for protein precipitates induced by a variety of more stressful conditions (e.g., high temperature, exposure to high or low pH, or addition of chaotropes) (*45*, *46*). Thus, it is not necessary to employ solution conditions that drastically perturb the native α-helical structure of rhGCSF in order to form an insoluble non-native aggregated state that is rich in intermolecular β-sheet. We speculate that the transition to β-sheet is a result of aggregate formation, and not due to the monomeric protein assuming a β-sheet "template" structure prior to assembly.

Thermodynamics of rhGCSF Unfolding. In the absence of sucrose, the estimates for ΔG_{unf}(25 °C) based on GdnHCl- and urea-induced unfolding curves were 8.4 and 10.0 kcal/mol, respectively. The value from the thermal unfolding corrected to 25 °C was 9.5 kcal/mol. The difference between ΔG_{unf}'s estimated by GdnHCl-induced unfolding and those estimated from urea- and thermally induced unfolding can be explained at least partially by salt effects. At pH 6.9, rhGCSF has 21 charged residues (*32*). The screening of electrostatic interactions between these groups caused by the high ionic strength of GdnHCl solutions under unfolding conditions (2.6−3.2 M GdnHCl) may affect estimates of ΔG_{unf}. Because urea is uncharged, no such interactions can impact the estimate of ΔG_{unf} obtained from unfolding curves. The close agreement between the value obtained from urea- and thermally induced unfolding curves documents that the latter method does provide accurate estimates of the thermodynamic parameters for rhGCSF unfolding. This conclusion is further supported by the highly linear van't Hoff plots (see Experimental Procedures). If aggregation or other irreversible processes were significantly affecting the estimates of ΔG_{unf} from thermal unfolding, nonlinearity should be apparent, especially at higher temperatures where the irreversible reactions would be expected to contribute more to the temperature-dependent change in the CD spectroscopic signal.

Effects of Sucrose. As demonstrated by thermally induced unfolding studies, addition of sucrose increases the thermodynamic stability of the native state of rhGCSF (Table 2). This is due to the preferential exclusion of sucrose from the surface of the protein, which favors the more compact native state over the greatly expanded unfolded state (*27*−*29*). The increases in enthalpy of unfolding as a function of sucrose concentration are modest and consistent with values obtained by Xie and Timasheff (*47*−*49*) for thermal unfolding of ribonuclease A in sorbitol and trehalose solutions. An increase in ΔH_m in the presence of these cosolvents can be explained by the increase in work required to expand the protein against an increased surface tension in these solutions (*50*). The small increase in ΔS_m may be due in part to sucrose-induced compaction of the time-averaged native state conformation, lowering the entropy of the native state relative to the effects of the sugar on the denatured state.

Consistent with this suggestion, sucrose reduces the rate of H−D exchange for rhGCSF (Figure 6). H−D exchange from the native state occurs as a result of the dynamic fluctuations that transiently break internal hydrogen bonds and expose backbone amides to solvent (*51*, *52*). In the presence of sucrose, the time-averaged conformation of rhGCSF is more compact, with the population of broken H-bonds at any instant in time reduced relative to that for protein in sucrose-free solutions (*17*). In other words, preferential exclusion favors lower entropy, less-expanded species within the native state ensemble and shifts the population of protein molecules away from aggregation-prone species (*17*, *19*). This result can explain the capacity of sucrose to inhibit protein aggregation (*16*). If the rate-limiting step for aggregation involves structurally expanded protein molecules as transition state species, the presence of sucrose will reduce their concentration, thereby slowing the aggregation reaction.

Role of the Observed Dimer. SE-HPLC indicates that, after an initial induction period, the population of reversible dimer decreases as the level of insoluble aggregates increases. Might this dimer be the precursor for insoluble aggregates of rhGCSF? One argument against this suggestion is the acceleration of the aggregation reaction noted at longer incubation times, despite decreasing dimer levels. Furthermore, the monomer−dimer equilibrium measured by SE-HPLC is unaffected by addition of sucrose, whereas the aggregation rate decreases 10-fold in the presence of 1 M sucrose. Also, second-derivative UV absorbance spectra (Figure 4C) show that exposure of tyrosine and tryptophan to solvent in the dimer is much less than that in the monomer. This observation indicates that dimer formation is due to the interaction of hydrophobic regions of monomer in which the above residues are found. Furthermore, the tyrosine solvent exposure in the dimer (observed at 1.5 h of incubation) was less than that for the precipitate. Under conditions where we observed aggregation, the dimer formed 3.5% of the total soluble protein, or about 0.05 mg/mL. Yet, when dimer was

concentrated nearly 3-fold (0.12 mg/mL) by pooling dimer fractions from an SE-HPLC system, no aggregates could be detected after 8 h of incubation under the same conditions. These arguments, combined with the observed reversibility of dimer formation, suggest that rhGCSF aggregation is not directly affected by dimerization of the native monomer.

Aggregation Kinetics of rhGCSF. The loss of native protein from solution initially follows second-order kinetics (Figure 3), and then accelerates (Figure 1A). Similar acceleration also has been observed for aggregation of interleukin 1β (*53*). Acceleration of rhGCSF aggregation is consistent with a mechanism whereby aggregates can be formed from a structurally perturbed monomer, M*, which can react irreversibly either with itself to form dimer, M_2, or with existing aggregates, M_x, to form larger aggregates, M_{x+1} (Scheme 1). Thus, as aggregation proceeds, aggregation levels increase, and the observed rate of loss of monomer increases:

Scheme 1

$$M \overset{K}{\rightleftharpoons} M^* \quad \text{(a)}$$

$$2M^* \overset{k}{\rightarrow} M_2 \quad \text{(b)}$$

$$M^* + M_x \rightarrow M_{x+1} \quad \text{(c)}$$

In this process, M_2 is a putative dimer that is distinct from the dimeric species that is observed to be in equilibrium with the native monomer. We cannot detect this particular dimer, likely because it is highly reactive (and thus found at very low concentrations), and even in the absence of reaction it would coelute with the "equilibrium" dimer on SE-HPLC. The reaction in Scheme 1c of expanded monomer with M_x, an aggregate of x monomer units, proceeds with a bimolecular rate constant k_x and provides the acceleration in aggregation over time that is observed in the experiments.

The decrease in initial aggregation reaction rates in the presence of sucrose is not solely due to the increased viscosity of sucrose solutions (Table 1). The viscosity of a 1 M sucrose solution is 2.6 times the viscosity of the sucrose-free solution, yet the initial reaction rate decreases by more than 10-fold. As noted above, an explanation for the enhanced inhibition over that expected due to viscosity effects is sucrose-induced thermodynamic shift of protein populations away from expanded, aggregation-prone state(s) toward the compact native monomer state.

Calculation of Surface Area Changes for Formation of Transition State Species. The change in surface area required to form a transition state species can be calculated from transition state theory using eq 2:

$$-RT\frac{\partial \ln K}{\partial \sigma} = \Delta a^* \quad (2)$$

where R is the gas constant, T is the temperature, σ is the surface tension of the solution, K is the equilibrium constant appearing in Scheme 1a, and Δa^* is the difference in partial molar surface areas between the M and M* states. The observed rate constant, k_{obs}, can be seen from Scheme 1 to be equal to kK^2, and the rate of aggregation $\nu = kK^2M^2 = k_{obs}M^2$. Assuming that the reaction to form M_2 from M* operates at the diffusion limit, the true second-order rate constant k is expected to be inversely proportional to viscosity, μ. Thus, we may modify eq 2 as follows:

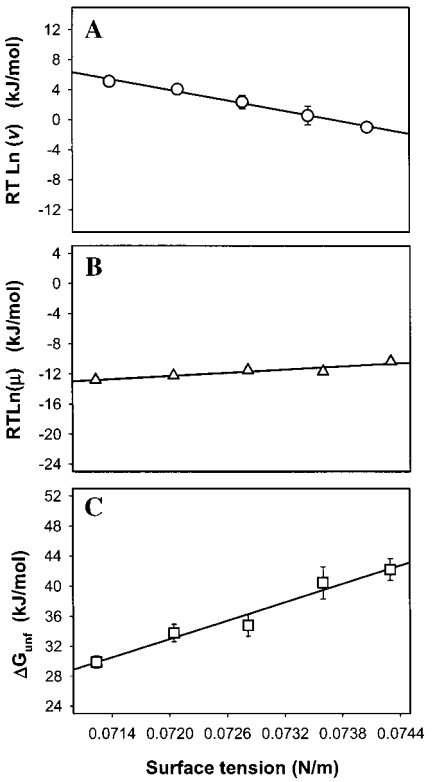

FIGURE 7: Partial molar surface area increase of rhGCSF monomer on formation of aggregation-competent transition and unfolded states. The variation in surface tension with sucrose concentration was obtained from Supran et al. (*60*). (A) RT ln (initial rate, ν) vs surface tension, σ; (B) RT ln (viscosity, μ) vs σ; (C) ΔG_{unf} at different sucrose concentrations, obtained from thermal unfolding experiments, vs surface tension. Half of the sum of the slopes of plots (A) and (B) provides the partial molar surface area change of the monomeric protein on formation of the aggregation-competent transition state, 1 nm^2/molecule. The slope of the plot (C) gives the partial molar surface area increase of rhGCSF on thermal unfolding, 6.5 nm^2/molecule. Data points represent the mean $\pm$ SD for triplicate samples except for plot (B), where the viscosity was estimated as described in Table 1.

$$-\frac{RT}{2}\left(\frac{\partial \ln k_{obs}}{\partial \sigma} + \frac{\partial \ln \mu}{\partial \sigma}\right) = \Delta a^* \quad (3)$$

Further, if initial rates of aggregation, ν_0, are measured at constant initial monomer concentration, Δa^* can be calculated as

$$-\frac{RT}{2}\left(\frac{\partial \ln \nu_0}{\partial \sigma} + \frac{\partial \ln \mu}{\partial \sigma}\right) = \Delta a^* \quad (4)$$

Figure 7A,B shows plots of RT ln ν_0 and RT ln μ, respectively, vs solution surface tension. From the slopes of these lines, Δa^*, the difference in partial molar surface area between the monomer and the aggregation transition state, was estimated to be 1 nm^2 per molecule. For comparison, the partial molar surface change upon unfolding, Δa_{unf}, can be calculated from

$$\frac{\partial \Delta G_{unf}}{\partial \sigma} = \Delta a_{unf} \quad (5)$$

A plot of ΔG_{unf} from the thermal unfolding experiments versus solution surface tension (Figure 7C) yields a value for Δa_{unf} of 6.5 nm^2 per molecule. Thus, the surface area increase for forming the aggregation-competent monomeric transition state from native monomer is 15% of that for unfolding of rhGCSF.

Diffusion-Limited Aggregation. The upper limit for a bimolecular reaction rate is the rate at which reactants can diffuse together, under pseudo-steady-state conditions. This rate can be estimated from Smoluchowski−Stokes−Einstein theory, which takes into account the effect of molecular size and solution viscosity on diffusivities and resulting reaction rates (*54*). According to this theory, the bimolecular reaction rate constant k can be expressed as

$$k = \frac{8RT}{3\mu} \quad (6)$$

The maximum attainable rate of reaction is k[reactant]^2. We may use this relationship together with our experimental estimates of equilibrium populations of various rhGCSF species to discern which species is most likely serving as the reactant for the rate-limiting step of aggregation. The species for which we have estimates of their equilibrium concentrations include the native monomer, the dimer detected by SE-HPLC in incubated samples, and the unfolded state. First, in the absence of sucrose, and at an overall protein concentration of 1.5 mg/mL, the calculated rate for diffusion-limited aggregation of native monomer is 5.4×10^6 mol L^{-1} day^{-1}. For the equilibrium dimer detected by SE-HPLC, the diffusion-limited rate is 8×10^2 mol L^{-1} day^{-1}, and the corresponding rate for unfolded monomer reacting at the diffusion limit is 5×10^{-4} mol L^{-1} day^{-1}. In comparison, the actual rate is 7.3×10^{-6} mol L^{-1} day^{-1}, which is approximately 8 orders of magnitude slower than the diffusion limit for dimer−dimer aggregation, supporting the argument that the observed dimer does not participate in the rate-limiting step of aggregation (Figure 8). The actual rate is closer to that predicted for diffusion-limited aggregation of the unfolded state, but this estimate does not adequately predict the slope of the aggregation rate versus sucrose concentration: diffusion-limited reaction rates overpredict the actual rate at low sucrose concentration (below 0.5 M) and underpredict the rate at sucrose concentrations above 0.5 M (Figure 8). Therefore, it is unlikely that the aggregation pathway of rhGCSF proceeds through the unfolded state. Furthermore, the predicted rate is almost 12 orders of magnitude slower than that predicted for the population of the native monomer. At 37 °C in the absence of sucrose, the predicted bimolecular rate constant for a diffusion-limited reaction (eq 6) is 9.9×10^9 M^{-1} s^{-1}. Assuming diffusion-limited reaction, the concentration of reactive species required to yield the experimental aggregation rate of 7.3×10^{-6} M day^{-1} is 9.2×10^{-11} M, compared to the concentration of native monomer used in our experiments of 7.9×10^{-5} M. Taken together, these results suggest that the reactive species for rhGCSF aggregation is most likely one that accounts for one out of every million molecules in the native state ensemble. Even though this species is rare, its levels are sufficient to drive substantial aggregation of the protein over a short time frame, relative to that for formation of non-native protein aggregates in vivo in human diseases or to the storage time (18−24 months) for pharmaceutical proteins.

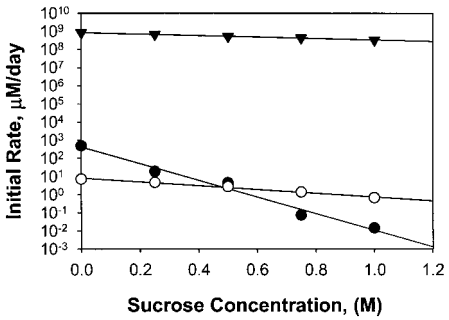

FIGURE 8: Comparison of the estimated diffusion limit for the aggregation rate of the equilibrium dimer and the experimentally observed rate of aggregation. The figure shows experimentally observed initial reaction rates of aggregation at different sucrose concentrations (open circles) in comparison with rates calculated from the Smoluchowski−Stokes−Einstein theory for diffusion-limited aggregation of the equilibrium dimer of rhGCSF (closed triangles) at those same sucrose concentrations. The initial reaction rates of the diffusion-limited aggregation of the unfolded states at different sucrose concentrations are also shown (closed circles). The diffusion-limit for aggregation was obtained by calculating the concentration of dimer from the monomer−dimer equilibrium constants K_d (Table 1), and then calculating the reaction rate as k*[dimer]^2, where k is the bimolecular rate constant from the Smoluchowski−Stokes−Einstein relation (eq 6). Values for viscosity for different sucrose concentrations were taken from Table 1. The large discrepancy in the observed rate vs that which would be predicted if the dimer directly participated in the aggregation reaction (closed triangles) suggests that the observed equilibrium dimer is not a direct participant in aggregation of rhGCSF.

Conclusions. Nonspecific thermodynamic stabilization by sucrose of the native state of proteins has been shown to inhibit aggregation of interleukin-1 receptor antagonist (*17*, *55*), interferon-γ (*16*, *21*), LDH (*56*), recombinant di-α-linked hemoglobin (*57*), and immunoglobulin light chains (*19*) in the presence of perturbing solutes, agitation, freezing, or elevated temperature. The current results show that, even in the absence of such stresses, nonspecific thermodynamic stabilizers can inhibit aggregation. Ligands that bind specifically and with high affinity to the native state are expected to offer even more pronounced protection against aggregation (*58*, *59*). This strategy should be applicable even under physiological conditions where the native state is already greatly favored thermodynamically.

ACKNOWLEDGMENT

We gratefully acknowledge Amgen Inc., for providing us with technical support for the project. We also acknowledge Dot Dill for her help with TEM.

REFERENCES

1. Hardy, J., and Gwinn-Hardy, K. (1998) *Science 282*, 1075−1078.
2. Koo, E. H., Lansbury, P. T., and Kelly, J. W. (1999) *Proc. Natl. Acad. Sci. U.S.A. 96*, 9989−9990.
3. Lansbury, P. T. (1999) *Proc. Natl. Acad. Sci. U.S.A. 96*, 3342−3344.
4. Harper, J. D., and Lansbury, P. T. (1997) *Annu. Rev. Biochem. 66*, 385−407.
5. Kyle, R. A. (1994) *Annu. Rev. Med. 45*, 71−77.
6. Cleland, J. F., Powell, M. F., and Shire, S. J. (1993) *Crit. Rev. Ther. Drug Carrier Syst. 10* (4), 307−377.
7. Manning, M. C., Patel, K., and Borchardt, R. T., (1989) *Pharm. Res. 6*, 903−918.

8. Carpenter, J. F., Kendrick, B. S., Chang, B. S., Manning, M. C., and Randolph, T. W. (1999) *Methods Enzymol. 309*, 236−255.
9. Fink, A. L. (1998) *Folding Des. 3*, R9−R23.
10. DeFellips, M. R., Alter, L. A., Pekar, A. H., Havel, H. A., and Brems, D. N (1993) *Biochemistry 32*, 1555−1562.
11. Kuznetsove, I. M., Biktahev, A. G., Khaitlina, S. Y., Vassilenko, K. S., Turoverov, K. K., and Uversky, V. N. (1999) *Biophys. J. 77*, 2788−2800.
12. Uversky, V. N., and Fink, A. K. (1998) *Biochemistry (Moscow) 63* (4), 456−462.
13. Arakawa, T., and Hsu, Y. R. (1987) *Biochemistry 26*, 5428−5432.
14. Kelly, J. W. (1998) *Curr. Opin. Struct. Biol. 8*, 101−106.
15. Colon, W., and Kelly, J. W. (1992) *Biochemistry 31*, 8654−8660.
16. Kendrick, B. S., Carpenter, J. F., Cleland, J. L., and Randolph, T. W. (1998) *Proc. Natl. Acad. Sci. U.S.A. 95*, 14142−14146.
17. Kendrick, B. S., Chang, B. S., Arakawa, T., Peterson, B., Randolph, T. W., Manning, M. C., and Carpenter, J. F. (1997) *Proc. Natl. Acad. Sci. U.S.A. 94*, 11917−11922.
18. Wetzel, R. (1997) *Adv. Protein Chem. 50*, 183−242.
19. Kim, Y. S., Wall, J. S., Meyer, J. D., Murphy, C., Randolph, T. W., Manning, M. C., Solomon, A., and Carpenter, J. F. (2000) *J. Biol. Chem. 275*, 1570−1574.
20. Kim, Y. S., Cape, S. P., Chi, E., Raffen, R., Wilkins-Stevens, P., Stevens, F. J., Manning, M. C., Randolph, T. W., Solomon, A., and Carpenter, J. F. (2001) *J. Biol. Chem. 276*, 1626−1633.
21. Webb, J. N., Webb, S. D., Cleland, J. L., Carpenter, J. F., and Randolph, T. W. (2001) *Proc. Natl. Acad. Sci. U.S.A. 98*, 7259−7264.
22. Wang, W. (1999) *Int. J. Pharm. 185*, 129−188.
23. Garcia-Perez, A., and Burg, M. (1991) *Physiol. Rev. 71*, 1081−1115.
24. Burg, M. B., and Peters, E. M. (1998) *Am. J. Physiol. 274*, F762−F765.
25. Wang, A., Robertson, A. D., and Bolen, D. W. (1995) *Biochemistry 34*, 15096−15104.
26. Liu, Y., and Bolen, D. W. (1995) *Biochemistry 34*, 12884−12891.
27. Timasheff, S. N. (1998) *Adv. Protein Chem. 91*, 355−432.
28. Arakawa, T., and Timasheff, S. N. (1985) *Biophys. J. 47*, 411−414.
29. Arakawa, T., and Timasheff, S. N. (1982) *Biochemistry 21*, 6536−6544.
30. Kolvenbach, C. G., Elliott, S., Sachdev, R., Arakawa, T., and Narhi, L. O. (1993) *J. Protein Chem. 12*, 229−236.
31. Narhi, L. O., Kenney, W. C., and Arakawa, T. (1991) *J. Protein Chem. 10*, 359−367.
32. Herman, A. C., Boone, T. C., and Lu, H. S. (1996) in *Formulation, Characterization, and Stability of Protein drugs* (Pearlman, R., and Wang, Y. J., Eds.) pp 303−328, Plenum Press, New York.
33. Ackland, C. E., Berndt, W. G., Frezza, J. E., Landgraf, B. E., Pritchard, K. W., and Ciardelli, T. L. (1991) *J. Chromatogr. 540*, 187−198.
34. Santoro, M. M., and Bolen, D. W. (1988) *Biochemistry 27*, 8063−8068.
35. Bolen, D. W., and Santoro, M. M. (1988) *Biochemistry 27*, 8069−8074.
36. Pace, C. N., and Shaw, K. L. (2000) *Proteins: Struct., Funct., Genet. Suppl. 4*, 1−7.
37. Pace, C. N. (1990) *Trends Biotechnol. 8*, 93−98.
38. Edelhoch, H., and Osborne, J. C., Jr. (1976) *Adv. Protein Chem. 30*, 183.
39. Dong, A., Huang, P., and Caughey, W. S. (1990) *Biochemistry 29*, 3303−3308.
40. Holien, J., and Marquesee, S. (1999) *Proc. Natl. Acad. Sci. U.S.A. 96*, 13674−13678.
41. Mach, H., and Middaugh, C. R. (1994) *Anal. Biochem. 222*, 323−331.
42. Ragone, R., Colonna, G., Balestrieri, C., Servillo, L., and Irace, G. (1984) *Biochemistry 23*, 1871−1875.
43. Servillo, L., Colonna, G., Balestrieri, C., Ragone, R., and Irace, G. (1982) *Anal. Biochem. 126*, 251−257.
44. Wang, A., Robertson, A. D., and Bolen, D. W. (1995) *Biochemistry 34*, 15096−15104.
45. Uversky, V. N., Karnoup, A. S., Khurana, R., Segel, D. J., Doniach, S., and Fink, A. L. (1999) *Protein Sci. 8*, 161−173.
46. Kendrick, B. S., Cleland, J. L., Lam, X., Nguyen, T., Randolph, T. W., Manning, M. C., and Carpenter, J. F. (1998) *J. Pharm. Sci. 87*, 1069−1076.
47. Xie, G., and Timasheff, S. N. (1997) *Protein Sci. 6*, 211−221.
48. Xie, G., and Timasheff, S. N. (1997) *Protein Sci. 6*, 222−232.
49. Xie, G., and Timasheff, S. N. (1997) *Biophys. Chem. 64*, 25−43.
50. Lee, J. C., and Timasheff, S. N. (1981) *J. Biol. Chem. 256*, 7193−7201.
51. Foord, R. L., and Leatherbarrow, R. J. (1998) *Biochemistry 37*, 2969−2978.
52. Raschke, T. M., and Marquesee, S. (1998) *Curr. Opin. Biotechnol. 9*, 80−86.
53. Gu, L. C., Erdos, E. A., Chiang, H., Calderwood, T., Tsai, K., Visor, G. C., Duffy, J., Hsu, W. C., and Foster, L. C. (1991) *Pharm. Res. 8*, 485−490.
54. Smoluchowski, M. (1917) *Z. Phys. Chem. 92*, 129.
55. Chang, B. S., Beauvais, R. M., Arakawa, T., Narhi, L. O., Dong, A., Apariso, D. I., and Carpenter, J. F. (1996) *Biophys. J. 71*, 3399−3406.
56. Hall, R. H., Jacobsen, M. P., and Winzor, D. J. (1995) *Biophys. Chem. 57*, 47−54.
57. Kerwin, B. A., Heller, M. C., Levin, S. H., and Randolph, T. W. (1998) *J. Pharm. Sci. 87*, 1062−1068.
58. Tjernberg, L. O., Lilliehook, C., Callaway, D. J. E., Naslund, J., Hahne, S., Thyberg, J., Terenius, L., and Nordstedt, C. (1997) *J. Biol. Chem. 272*, 12601−12605.
59. Petersen, S. A., Klabunde, T., Lashuel, H. A., Purkey, H., Sacchettini, J. C., and Kelly, J. W. (1998) *Proc. Natl. Acad. Sci. U.S.A. 93*, 15051−15056.
60. Supran, M. K., Acton, J. C., Howell, A. J., and Saffle, R. L. (1971) *J. Milk Food Technol. 34*, 584−585.

BI012006M